the *h0l* spectra of these four peroxides are very similar, the projected molecular arrangement is that shown in Fig. 4. Although ordered crystal structures with an alternating arrangement of iodine and bromine (chlorine) atoms along the lattice vector **c** are not consistent with the absence of *h0l* spectra with *l* odd, disordered structures in which the heavy atoms sites are randomly occupied by iodine and bromine (I*d*) or iodine and chlorline (I*e*) atoms can not be excluded. However, in no case have diffuse spectra or interlayer streaking been observed.

The near equivalence of these spectra is in striking contrast to the greatly different X-ray spectra which the respective peroxide crystals develop simply upon standing! Whereas single crystals of (I*a*), (I*d*) and (I*e*) are transformed to solids which exhibit clearly different single-crystal diffraction spectra, decomposed single crystals of (I*b*) exhibit only the diffuse scattering characteristic of amorphous solids.

The authors wish to thank the United States Air Force Office of Scientific Research for financial support of this research (Grant No. AF-AFOSR-1059-67) and the National Institutes of Health for a predoctoral fellowship to J. C. C.

References

CATICHA-ELLIS, S. & ABRAHAMS, S. C. (1968). *Acta Cryst.* B**24**, 277.
FERGUSON, G. & SIM, G. A. (1962). *Acta Cryst.* **15**, 346.
GLASSER, L. S. D., GLASSER, F. P. & TAYLOR, H. F. W. (1962). *Quart. Rev. Chem. Soc. Lond.* **16**, 343.
International Tables for X-ray Crystallography (1962). Vol. III. Birmingham: Kynoch Press.
JEFFREY, G. A., MCMULLAN, R. K. & SAX, M. (1964). *J. Amer. Chem. Soc.* **86**, 949.
KATZ, L. & MEGAW, H. D. (1967). *Acta Cryst.* **22**, 639.
LEFFLER, J. E., FAULKNER, R. D. & PETROPOULOS, C. C. (1958). *J. Amer. Chem. Soc.* **80**, 5434.
LONSDALE, K., NAVE, E. & STEPHENS, J. F. (1966). *Phil. Trans.* A**261** (1114), 1.
MOROSOFF, N., MORAWETZ, H. & POST, B. (1965). *J. Amer. Chem. Soc.* **87**, 3035.
SAX, M. & MCMULLAN, R. K. (1967). *Acta Cryst.* **22**, 281.
WILSON, A. J. C. (1942). *Nature, Lond.* **150**, 152.

Acta Cryst. (1970). B**26**, 2008

The Crystal Chemistry of the Rare Earth Orthoferrites

BY M. MAREZIO, J. P. REMEIKA AND P. D. DERNIER

Bell Telephone Laboratories, Incorporated, Murray Hill, New Jersey, U.S.A.

(*Received* 24 *October* 1969)

The structural arrangements of the rare earth orthoferrites (from Pr to Lu) have been investigated by refining the respective crystal structures from X-ray diffraction data. It has been found that the distortion of the oxygen iron octahedra is small and almost constant when proceeding from $LuFeO_3$ to $SmFeO_3$. It begins to decrease at $NdFeO_3$, but even for $PrFeO_3$ it is of the same order of magnitude as in $LuFeO_3$. On the contrary, the oxygen polyhedra around the rare earth atoms are very distorted and their distortion varies appreciably across the series. The approximation that the coordination number of the rare earths is eight appears to be still valid. However, the data indicate that this is a good approximation only between $TbFeO_3$ and $NdFeO_3$. In fact, between $DyFeO_3$ and $LuFeO_3$ the seventh and eighth rare earth–oxygen distances increase while the radii of the rare-earths decrease. This indicates that for these compounds the seventh and eighth nearest oxygen atoms are becoming second-nearest neighbors. The ninth oxygen atom is a second-nearest neighbor throughout the series. Its distance from the rare earth decreases while the radii of the rare earths increase. At $PrFeO_3$ this distance begins to drop quite drastically so that at $LaFeO_3$ this oxygen atom cannot be considered to be a second-nearest neighbor. In this compound the difference between the eighth value, 2·805 Å, and the ninth, 3·041 Å, is 0·236 Å which is not large enough to assume that the coordination of the La^{3+} ions is eight. The arrangements of $InCrO_3$ and $InGaO_3$, which crystallize with the orthorhombic perovskite structure under high pressure, are discussed. In addition the possibility of synthesizing In_2O_3 with a perovskite-like arrangement under high pressure is proposed.

Introduction

The rare earth orthoferrites are known to crystallize with the orthorhombic distortion of the perovskite structure, which is a common arrangement for many ABO_3 compounds. For instance, the rare-earth orthochromites, orthovanadites, orthorhodites and orthoaluminates (from Sm to Lu) have been reported to be isostructural with $GdFeO_3$, which is considered the prototype of this series. In the cubic perovskite structure [see Fig. 1(*a*)] the *A* cations are surrounded by 12 equidistant oxygen ions, whereas the *B* cations are surrounded by an oxygen octahedron. In the orthorhombic distortion [see Fig. 1(*b*)] the *A* cations and the oxy-

gen ions are displaced from their cubic positions. Consequently the 12 oxygen polyhedra around the A cations are quite distorted, so that the 12 distances A–O vary over a large range. Also the oxygen octahedra around the B cations are distorted, but their distortion is far less than that of the polyhedra around the A cations. For instance, in $YFeO_3$ Coppens & Eibschütz (1965) found that the Y–O distances vary from 2·24 to 3·58 Å, whereas the Fe–O distances vary from 2·00 to 2·04 Å.

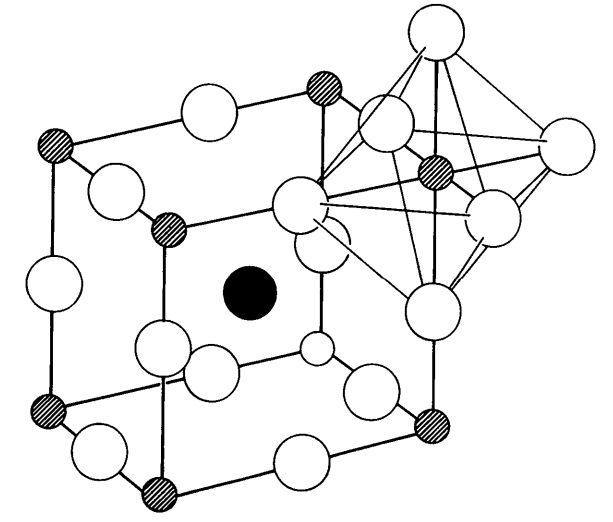

(*a*)

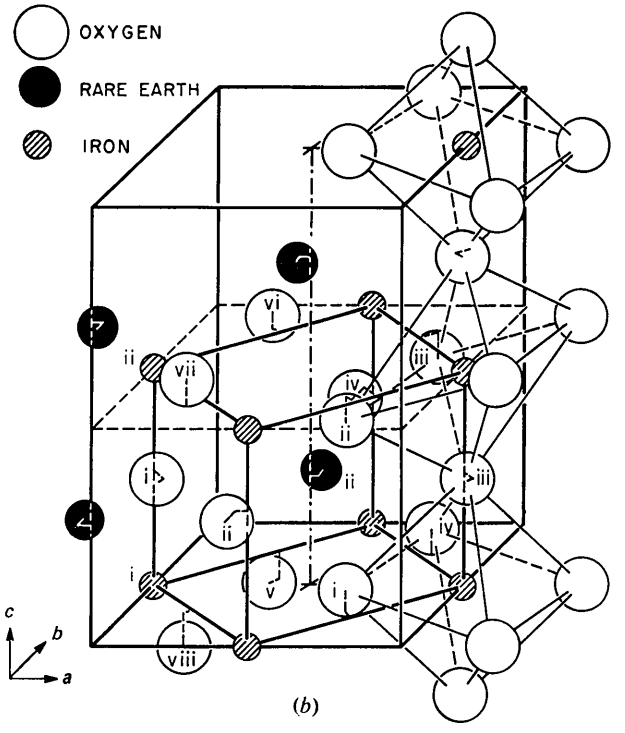

(*b*)

Fig. 1. Unit cell of (*a*) the 'ideal' cubic perovskite structure, (*b*) the orthorhombic perovskite-like structure.

A common feature of the rare earth orthoferrites, orthogallates (Marezio, Remeika & Dernier, 1968), orthochromites, orthovanadites and orthorhodites, is the variation of the lattice parameters of these compounds across the rare-earth series. The a and c parameters increase smoothly on going from Lu to La, whereas the b parameter has an unexpected behavior. It goes through a maximum at about Dy–Tb–Gd. We thought that this anomalous behavior could be explained if one considers the effect of the variation of the size of the A cation on the first nearest oxygen atoms together with the effect of the same variation on the second nearest oxygen atoms. Among the twelve rare-earth–oxygen distances in these compounds one can distinguish 8 first-nearest neighbors and 4 second-nearest neighbors. As the radius of the rare earth increases, the distances between the first-nearest oxygen atoms and the rare earth increase whereas the distances between the second-nearest oxygen atoms and the rare earth would decrease. Therefore the b parameter increases on going from Lu to Gd because in this region the first effect is the predominant one, whereas from Gd to La the second effect would be predominant. The decrease of the distances between the second-nearest oxygen atoms and the rare-earth as the radius of the A cations increases, would be due to the decrease of the screening effect of the first-nearest oxygen atoms on the second-nearest oxygen atoms. We thought also that as a consequence of the decrease of the distances between the second-nearest oxygen atoms and the rare earth, the coordination of the A cations would vary across the series.

In order to determine in detail the coordination of the rare earth in these compounds, the structural refinement of the rare-earth orthoferrites, $REFeO_3$ with RE = Pr–Lu has been undertaken from single-crystal X-ray data. The refinement of $LaFeO_3$ will be reported later as an attempt has been made to refine its structure from a twinned crystal. Since the structure of $LaFeO_3$ is nearly cubic, it is not possible to grow untwinned crystals of $LaFeO_3$. Actually the twinning is present also in $PrFeO_3$ and in $NdFeO_3$, but in these cases it is negligible.

Crystal growth

Prior work had shown that when rare-earth orthoferrites are crystallized from a molten lead salt, a considerable amount of the rare earth is substituted by lead (Remeika & Kometani, 1968). For this reason a solvent, or flux, was sought which would not be incorporated into the structure. It was felt that a potassium compound might be suitable because the large size of the K^+ ion would prevent its entering the orthoferrite structure. To this end, mixtures of K_2CO_3 and B_2O_3 were tried as a solvent. (We had determined from previous work that boron does not enter the structure.)

Starting materials were all of the ultra-pure variety. Mass spectrographic analysis of the rare-earth oxides

showed that the aggregate of all other rare earths, in any given oxide was <5p.p.m. Emission spectroscopic analysis of all materials used gave a total common impurity content of <10 p.p.m. A typical run consisted of the following amounts: $RE_2O_3=2{\cdot}50$, $Fe_2O_3=2{\cdot}00$, $K_2CO_3=13{\cdot}82$, $B_2O_3=6{\cdot}96$ g. These were weighed into a 100 cc platinum crucible, covered with a platinum lid, and placed in a horizontally loaded, resistively fired furnace at 1300°C. This temperature was maintained for about 2 hours to affect solution. Controlled cooling

Table 1. *Crystal data*

	a	*b*	*c*	*R* (mm)	μR	Orientation	N(1)	N(2)
Pr*	5·482 Å	5·578 Å	7·786 Å	0·095	2·49	[010]	1032	710
Nd*	5·453	5·584	7·768	0·100	2·79	[100]	1082	742
Sm*	5·400	5·597	7·711	0·107	3·36	[100]	981	738
Eu*	5·372	5·606	7·685	0·070	2·32	[010]	1014	698
Gd*	5·349	5·611	7·669	0·055	1·96	[100]	998	645
Tb†	5·326	5·602	7·635	0·096	3·62	[100]	996	743
Dy†	5·302	5·598	7·623	0·092	3·70	[100]	989	754
Ho†	5·278	5·591	7·602	0·076	3·24	[100]	979	673
Er†	5·263	5·582	7·591	0·104	4·70	[001]	968	727
Tm†	5·251	5·576	7·584	0·098	4·66	[001]	970	711
Yb†	5·233	5·557	7·570	0·085	4·32	[010]	953	661
Lu†	5·213	5·547	7·565	0·073	3·90	[010]	957	632

* The limits of error of the lattice parameters of these orthoferrites are $\pm 0{\cdot}001$ Å.
† For these lattice parameters Eibschütz (1965) gives $\pm 0{\cdot}003$ Å.

N(1) represents the number of reflections measured.
N(2) represents the number of reflections observed.

Table 2. *Final positional parameters and discrepancy factors*

		Pr	Nd	Sm	Eu	Gd	Tb
S.F.		0·844 (3)	0·933 (4)	1·044 (3)	0·549 (2)	0·409 (1)	0·928 (3)
$C\times 10^3$		0·32 (2)	0·35 (2)	0·41 (2)	0·37 (2)	0·33 (2)	0·33 (2)
RE	*x*	0·99097 (4)	0·98931 (4)	0·98688 (3)	0·98555 (5)	0·98444 (5)	0·98403 (3)
	y	0·04367 (5)	0·04881 (5)	0·05666 (3)	0·06012 (4)	0·06284 (6)	0·06408 (3)
	z	(0·25)	—	—	—	—	—
Fe	*x*	(0·00)	—	—	—	—	—
	y	(0·50)	—	—	—	—	—
	z	(0·00)	—	—	—	—	—
O(1)	*x*	0·0817 (7)	0·0876 (7)	0·0947 (6)	0·0978 (7)	0·1005 (10)	0·1035 (6)
	y	0·4788 (9)	0·4759 (8)	0·4710 (6)	0·4680 (7)	0·4672 (11)	0·4640 (6)
	z	(0·25)	—	—	—	—	—
O(2)	*x*	0·7075 (5)	0·7052 (5)	0·7004 (4)	0·6977 (5)	0·6957 (6)	0·6950 (4)
	y	0·2919 (5)	0·2936 (5)	0·2992 (4)	0·3006 (5)	0·3016 (6)	0·3026 (4)
	z	0·0437 (5)	0·0462 (4)	0·0497 (3)	0·0506 (4)	0·0506 (4)	0·0538 (3)
N		690	723	720	676	627	736
R		0·025	0·028	0·023	0·022	0·024	0·019
wR		0·042	0·042	0·033	0·030	0·034	0·031

		Dy	Ho	Er	Tm	Yb	Lu
S.F.		0·866 (3)	0·653 (2)	1·013 (3)	1·002 (4)	0·775 (3)	0·596 (2)
$C\times 10^3$		0·34 (2)	0·33 (3)	0·69 (5)	0·79 (5)	0·88 (6)	0·65 (5)
RE	*x*	0·98293 (4)	0·98219 (4)	0·98155 (4)	0·98104 (5)	0·98064 (5)	0·98003 (4)
	y	0·06648 (4)	0·06801 (5)	0·06913 (4)	0·06913 (4)	0·07076 (5)	0·07149 (5)
	z	—	—	—	—	—	—
Fe	*x*	—	—	—	—	—	—
	y	—	—	—	—	—	—
	z	—	—	—	—	—	—
O(1)	*x*	0·1060 (8)	0·1091 (9)	0·1137 (8)	0·1148 (9)	0·1169 (11)	0·1199 (10)
	y	0·4624 (7)	0·4605 (8)	0·4594 (7)	0·4559 (8)	0·4537 (12)	0·4539 (10)
	z	—	—	—	—	—	—
O(2)	*x*	0·6930 (5)	0·6924 (5)	0·6910 (5)	0·6907 (6)	0·6886 (6)	0·6893 (6)
	y	0·3049 (5)	0·3052 (6)	0·3059 (5)	0·3057 (6)	0·3077 (7)	0·3071 (7)
	z	0·0549 (4)	0·0560 (5)	0·0573 (4)	0·0587 (5)	0·0599 (6)	0·0621 (5)
N		734	656	716	695	643	615
R		0·023	0·022	0·023	0·028	0·029	0·022
wR		0·034	0·033	0·036	0·038	0·040	0·032

N=number of reflections used in the refinement, $R=\Sigma|\Delta F|/\Sigma|F_o|$, $wR=[\Sigma(w^{1/2}\Delta F)^2/\Sigma(w^{1/2}F_o)^2]^{1/2}$.

Table 3. *Final thermal parameters* ($\times 10^4$)

		Pr	Nd	Sm	Eu	Gd	Tb	Dy	Ho	Er	Tm	Yb	Lu
RE	β_{11}*	43·4 (7)	49·6 (7)	56·0 (6)	43·0 (6)	45·9 (7)	44·0 (5)	43·3 (6)	46·8 (6)	45·4 (7)	53·4 (7)	51·2 (8)	48·0 (6)
	β_{12}	36·8 (7)	44·5 (7)	45·2 (6)	28·4 (5)	34·6 (6)	30·2 (5)	29·7 (6)	33·3 (6)	44·1 (6)	44·2 (7)	44·2 (7)	33·5 (6)
	β_{33}	19·3 (4)	20·5 (4)	24·3 (3)	19·6 (3)	23·0 (3)	19·3 (3)	20·8 (3)	21·5 (3)	24·3 (3)	30·1 (4)	26·2 (4)	25·2 (3)
	β_{12}	−4·5 (6)	−3·9 (5)	−4·6 (3)	−3·8 (4)	−4·3 (7)	−4·6 (3)	−4·2 (3)	−3·2 (4)	−3·3 (3)	−4·0 (4)	−3·3 (5)	−1·6 (5)
	β_{13}†	(0·0)	—	—	—	—	—	—	—	—	—	—	—
	β_{23}	(0·0)	—	—	—	—	—	—	—	—	—	—	—
Fe	β_{11}	34 (2)	44 (1)	53 (1)	38 (1)	43 (3)	41 (1)	40 (1)	45 (2)	42 (2)	53 (2)	49 (2)	49 (2)
	β_{22}	29 (2)	42 (2)	44 (1)	31 (1)	35 (2)	32 (1)	35 (2)	36 (2)	39 (2)	49 (2)	56 (2)	39 (2)
	β_{33}	18 (1)	19 (1)	22 (1)	17 (1)	20 (1)	16 (1)	16 (1)	18 (1)	20 (8)	25 (1)	21 (1)	21 (1)
	β_{12}	−1 (1)	−1 (1)	0 (1)	−1 (1)	−2 (2)	−1 (1)	−2 (1)	0 (1)	−0 (1)	0 (1)	2 (2)	−2 (2)
	β_{13}	0 (1)	0 (1)	0 (1)	0 (1)	1 (1)	0 (1)	1 (1)	0 (1)	−1 (1)	0 (9)	1 (1)	0 (1)
	β_{23}	1 (1)	2 (1)	1 (1)	2 (1)	2 (1)	2 (1)	3 (1)	2 (1)	1 (1)	2 (1)	4 (1)	1 (1)
O(1)	β_{11}	65 (8)	65 (7)	62 (2)	71 (8)	75 (11)	72 (8)	81 (9)	72 (10)	76 (11)	85 (13)	85 (13)	79 (11)
	β_{22}	57 (9)	70 (10)	80 (7)	43 (9)	73 (14)	57 (7)	44 (7)	39 (10)	42 (8)	78 (10)	97 (15)	61 (11)
	β_{33}	17 (4)	19 (4)	18 (3)	14 (4)	13 (5)	14 (3)	12 (3)	25 (5)	17 (4)	29 (5)	17 (6)	16 (5)
	β_{12}	2 (7)	4 (6)	2 (5)	−4 (6)	16 (9)	−3 (5)	−3 (6)	−14 (7)	−12 (6)	−20 (8)	−27 (11)	−19 (9)
	β_{13}	(0·0)	—	—	—	—	—	—	—	—	—	—	—
	β_{23}	(0·0)	—	—	—	—	—	—	—	—	—	—	—
O(2)	β_{11}	56 (5)	66 (5)	66 (4)	52 (5)	59 (7)	54 (4)	56 (6)	51 (5)	51 (5)	62 (6)	57 (7)	61 (6)
	β_{22}	31 (5)	49 (6)	54 (5)	32 (5)	32 (7)	36 (4)	42 (5)	50 (7)	49 (6)	56 (6)	54 (8)	56 (7)
	β_{33}	34 (3)	30 (3)	33 (2)	30 (3)	35 (5)	27 (2)	24 (3)	30 (4)	30 (3)	41 (4)	37 (5)	24 (4)
	β_{12}	−4 (5)	−11 (5)	−7 (3)	−8 (4)	−13 (6)	−9 (3)	−12 (4)	−11 (5)	−11 (4)	−9 (5)	−12 (6)	−6 (6)
	β_{13}	2 (3)	4 (3)	6 (2)	7 (3)	4 (4)	3 (2)	7 (3)	3 (4)	3 (3)	0 (4)	12 (4)	6 (4)
	β_{23}	−4 (4)	−2 (4)	−2 (3)	−4 (3)	−5 (5)	−4 (3)	−6 (3)	−5 (4)	−13 (3)	−12 (4)	−13 (5)	−14 (4)

* The anisotropic thermal parameters are the coefficients in the expression $\exp[-(\beta_{11}h^2+\beta_{22}k^2+\beta_{33}l^2+2\beta_{12}hk+2\beta_{13}hl+2\beta_{23}kl)]$

† By symmetry $\beta_{13}=\beta_{23}=0$ for RE and O(1).

Table 4. *Observed and calculated structure factors*

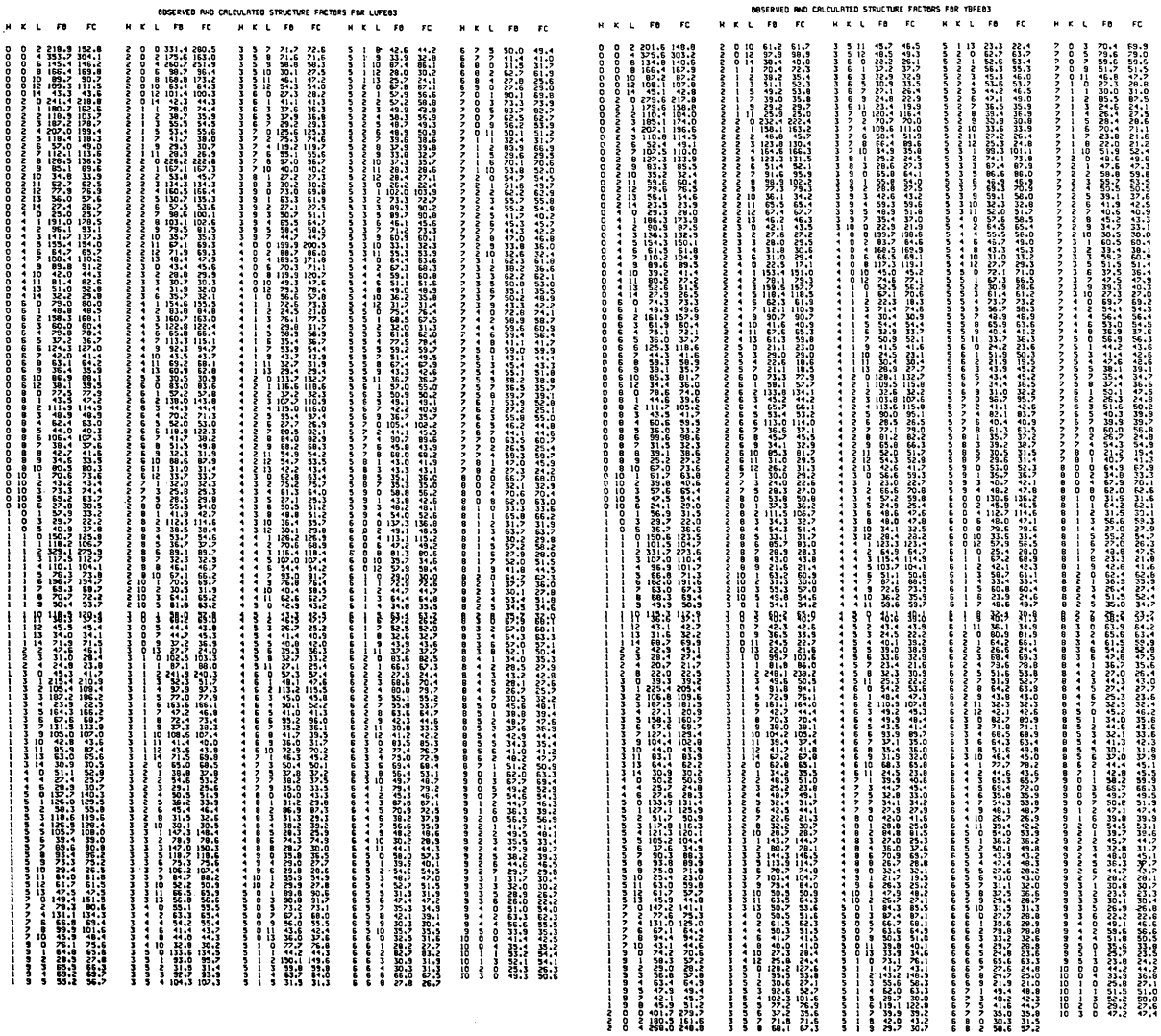

at a rate of about 5°C.hr^{-1} was then started and continued down to about 600°C. At this temperature the crucibles were removed from the furnace and allowed to cool quickly to room temperature. Extraction of the crystals from the solidified potassium borate glass was achieved by immersing the crucible in hot dilute HNO_3:H_2O with a volume ratio of approximately 1:8.

It should be made clear that we made no attempt to refine the process, since very small crystals satisfied requirements for the single-crystal X-ray refinement. The largest crystal (all were more or less cube shaped) was about 0·5 mm on a cube edge. Finally, the crystals were analyzed by the atomic absorption technique and found to be within 2% of stoichiometry for $REFeO_3$. Potassium was sought by emission spectroscopic analysis and found to be less than 0·005% by weight, which is the lowest limit of detectability for the instrument used.

Crystal data

We have recently confirmed (Marezio, Remeika & Dernier, 1970) that the structure of the rare-earth orthoferrites as determined by X-ray diffraction methods should be described in space group symmetry *Pbnm* as suggested by Geller (1956) and by Bertaut & Forrat (1956). (A nonstandard orientation of *Pnma* was chosen simply in keeping with historical precedent.) There are four formula units per unit cell. The four rare-earth atoms are in the special positions 4(*c*) $(x,y,\frac{1}{4})$, the four iron atoms are in special positions 4(*b*) $(0,\frac{1}{2},0)$; of the twelve oxygen atoms, four are in the special positions 4(*c*) $(x,y,\frac{1}{4})$ and eight in the general positions. The lattice parameters *a*, *b* and *c* of the rare-earth orthoferrites are reported in Table 1. The values from Tb to Lu are those determined by Eibschütz (1965), whereas the val-

Table 4 (*cont.*)

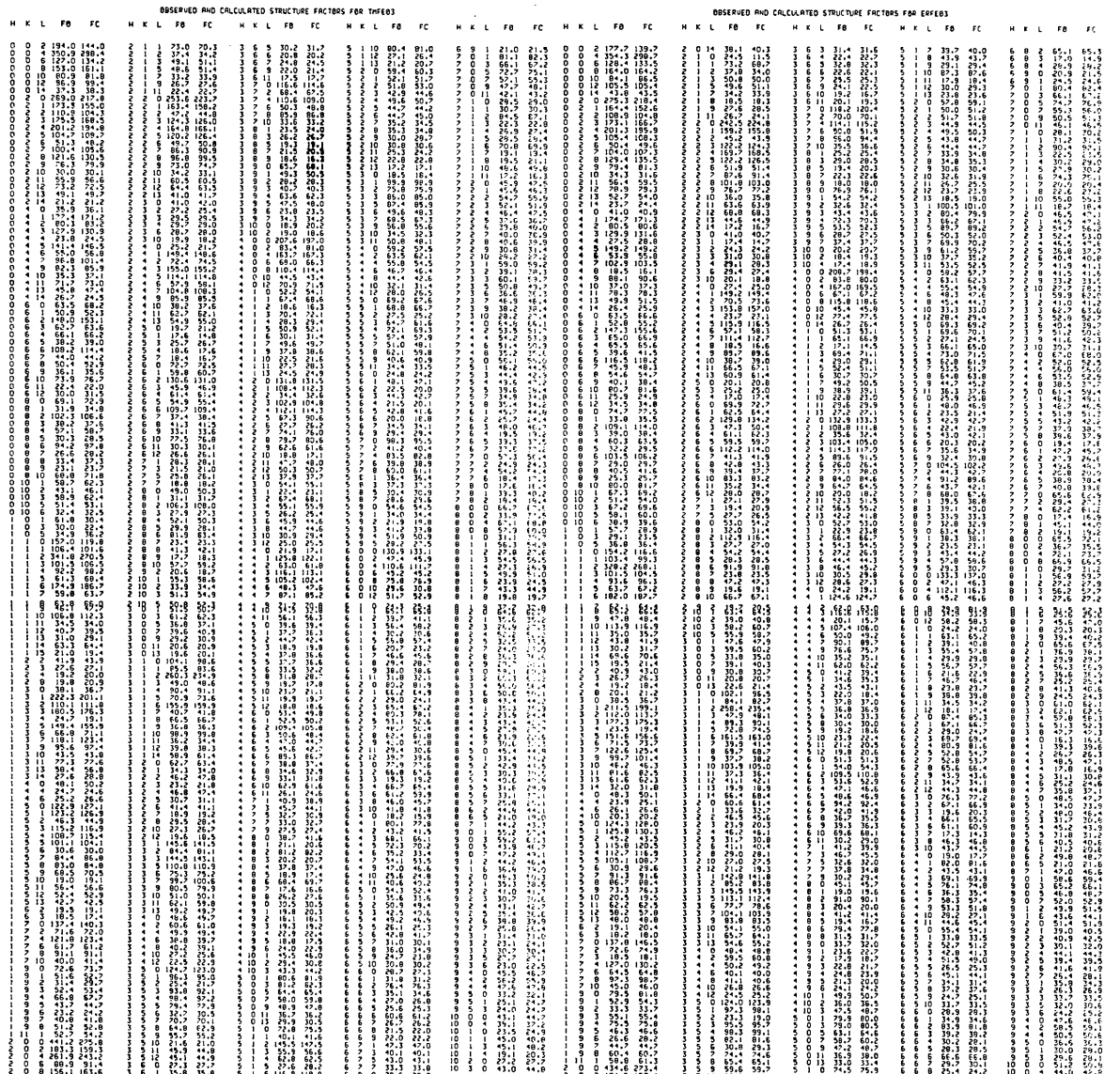

ues from Gd to Pr are new values. They were redetermined because the values previously reported were obtained by using orthoferrites containing lead (Remeika & Kometani, 1968). Samples of $REFeO_3$ were prepared by the ceramic method from the oxides RE_2O_3 and Fe_2O_3 of the same purity as those used to prepare single crystals. The X-ray powder photographs were taken at room temperature with a Norelco camera of 114·6 mm diameter and V-filtered Cr radiation ($K\alpha_1 =$ 2·28962 and $K\alpha_2 = 2{\cdot}29352$ Å). The final lattice parameters were obtained by accurate measurement of the 2θ values for at least ten reflections in the back-reflection region and by the least-squares refinement program of Mueller, Heaton & Miller (1960).

Intensity measurements

All intensity measurements were made with a General Electric paper-tape controlled, X-ray three-circle diffractometer. Mo K radiation was used together with a single Zr foil filter in the diffracted beam tunnel. A scintillation counter was used as the detection system. The specimens were spheres or ellipsoids which were approximated to spheres. Their average radii and orienta-

Table 4 (*cont.*)

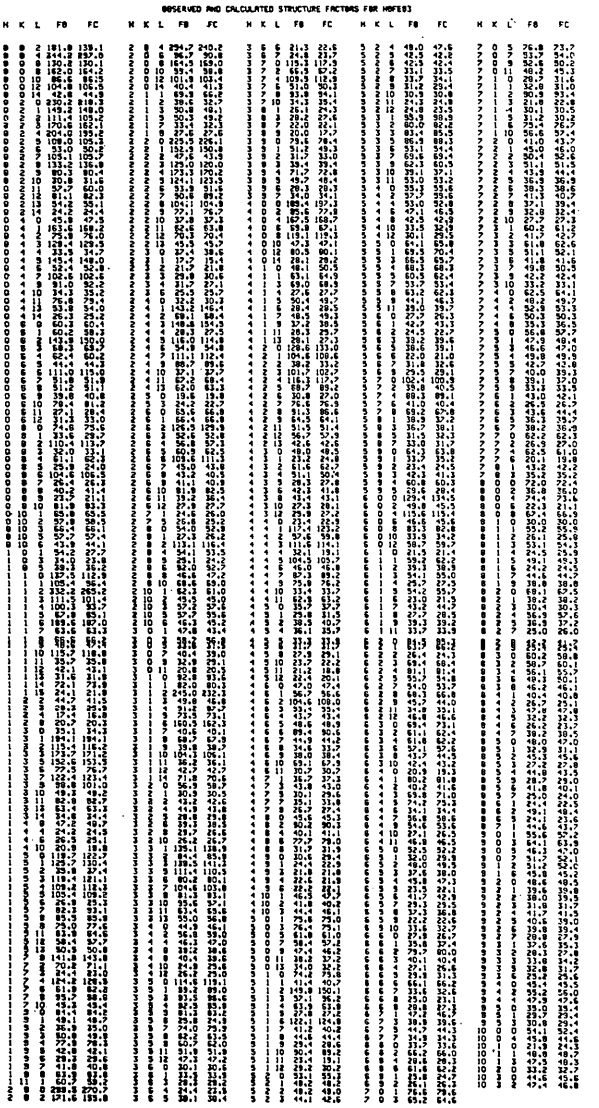

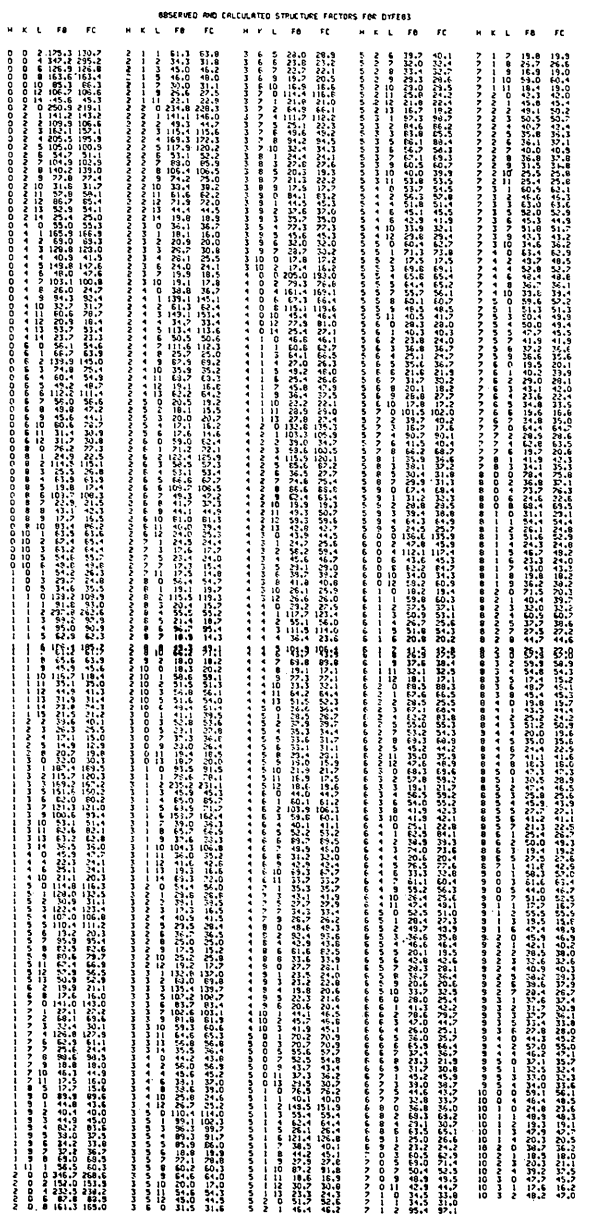

tions with respect to the φ axis of the goniostat are reported in Table 1. The integrated intensities were obtained with the stationary-crystal stationary-counter technique and single filter. The background was measured $\pm 2°$ of 2θ off the peak itself and the average was subtracted from the peak height. The take-off angle was 8°.

In the past several years a large quantity of intensity data have been collected with our present diffractometer under various experimental conditions and for many crystals of various sizes. It has been found that the integrated intensity can be accurately measured with the stationary-crystal stationary-counter technique provided that a small crystal (linear dimensions $<0{\cdot}3$ mm) and a large take-off angle are used. As long as the central segment of the focal spot completely bathes the sample, one could be sure of the constancy of the incident beam intensity.

For the $REFeO_3$ series all reflections having $2\theta \leq 90°$ included in the upper hemisphere were measured The total number of independent reflections measured for each rare-earth orthoferrite is given in the seventh column of Table 1. Those reflections for which the peak height was not at least twice as much as the background

Table 4 (*cont.*)

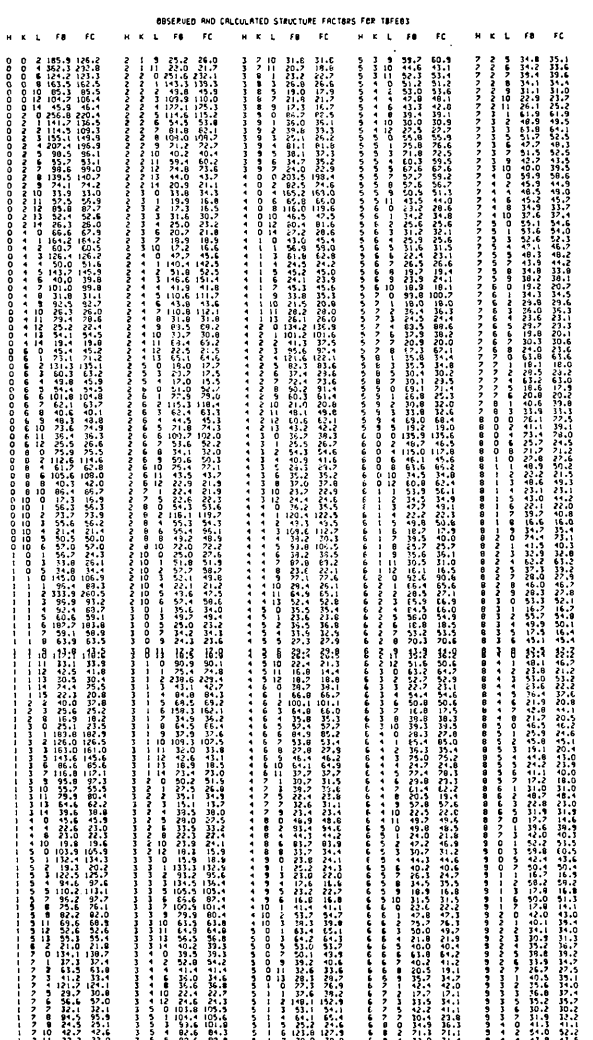

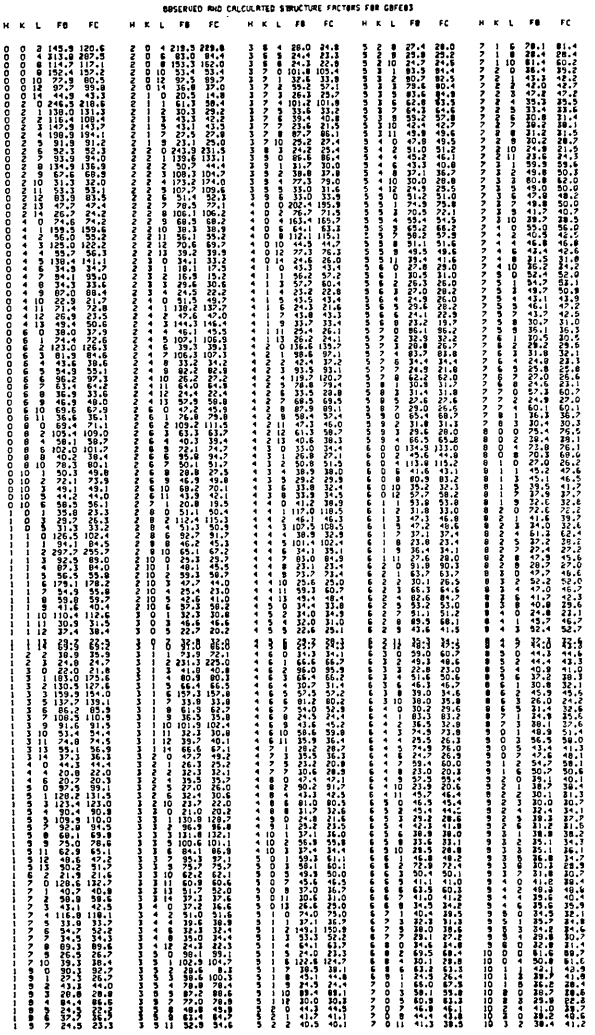

were regarded as unobserved. The number of observed reflections is given in the eighth column of Table 1. The integrated intensities were converted to structure factors by applying the Lorentz–polarization and absorption corrections.

Refinements

The refinements of the structures were carried out with the refinement program of Prewitt (1966*a*). In this program the function minimized is $\sum w||F_o|-|F_c||^2$. Each observed structure factor was weighted by $w=1/\sigma^2$ where $\sigma=2{\cdot}5$ when $|F|\leq 25$ and $\sigma=0{\cdot}1|F|$ when $|F|>25$, with the exception of those reflections for which $2\theta\leq 2\theta(004)$. Because of high background errors these reflections were excluded from the refinements. In each case the number of excluded reflections was less than 20. The atomic scattering tables (for neutral atoms) and the real and imaginary anomalous dispersion coefficients were taken from the values reported by Cromer & Waber (1965) and by Cromer (1965) respectively. The starting values for the positional parameters were the

Table 4 (*cont.*)

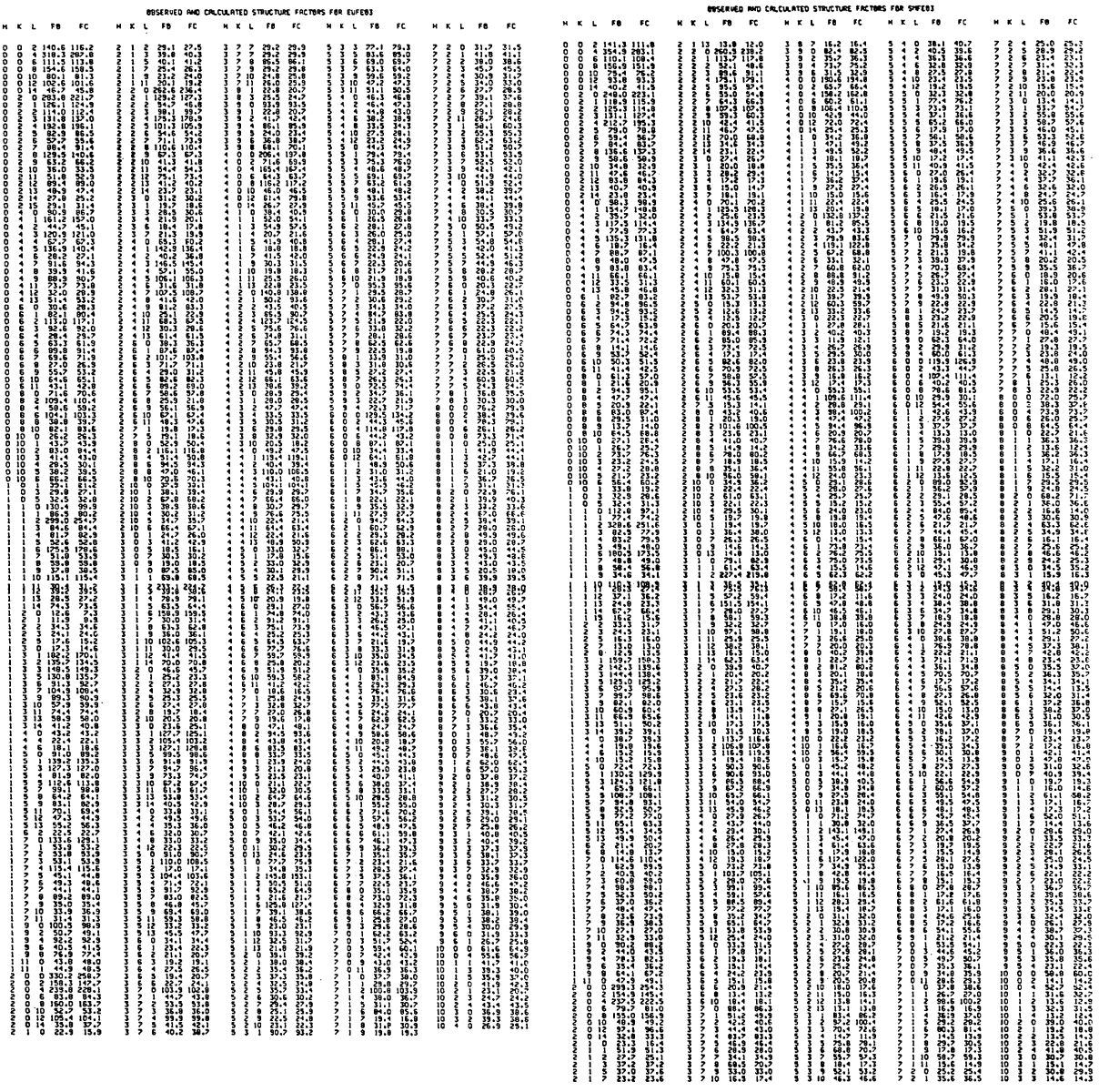

values given by Coppens & Eibschütz (1965) for $YFeO_3$. A value of 0·4 Å^2 was assumed for the isotropic temperature factors of the four atoms of the asymmetric unit. The secondary extinction correction was applied by using the Zachariasen (1963) formula. The value of the C coefficient was refined together with the positional and thermal parameters. After three cycles during which convergence was attained, anisotropic temperature factors were introduced. The final positional and thermal parameters are reported in Tables 2 and 3. A comparison between observed and calculated structure factors is shown in Table 4, where F_c represents the calculated scattering amplitude per unit cell.

In order to determine how much a departure from sphericity would affect the final refinements, two absorption corrections were carried out for one of the worst cases. This specimen was a crystal of $NdFeO_3$ which had a prismatic habit ground into a rotation ellipsoid whose principal axes coincided with the directions **a**, **b** and **c** of the crystal. The values, as measured with an optical comparator with Polaroid film cassette and 100× magnification, were found to be: $r(a)=0{\cdot}102$, $r(b)=0{\cdot}095$ and $r(c)=0{\cdot}102$ mm. The absorption

Table 4 (*cont.*)

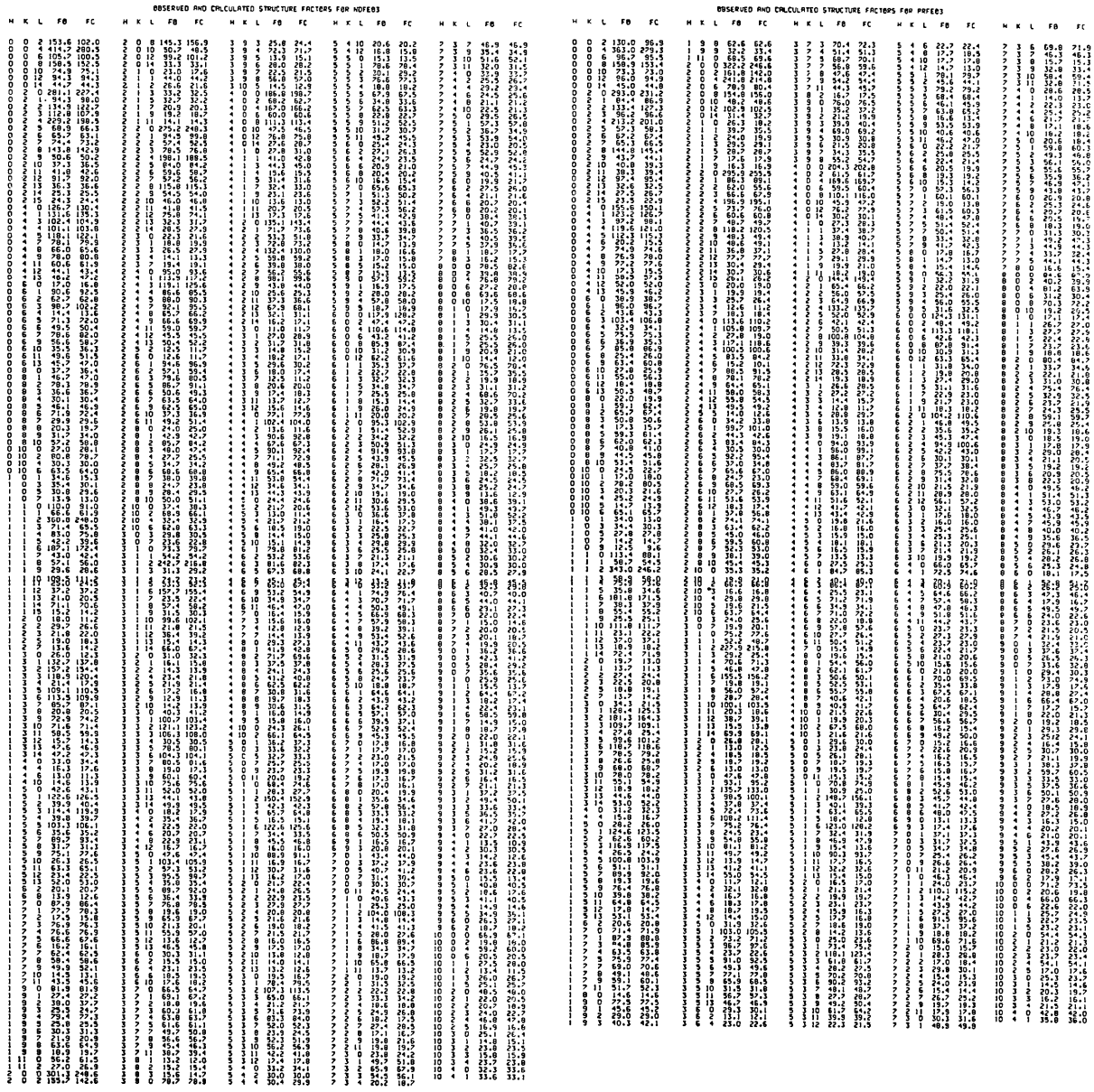

correction for the ellipsoidal shape was calculated numerically by using a program written by C. T. Prewitt (1966*b*). This program was modified in order to use the numerical integration method of Gauss. The structural refinement based on these data yielded positional parameters that did not differ significantly from the refinement based on data in which a spherical sample shape was assumed. In fact the positional parameters did not vary more than $\frac{1}{4}$ of one standard deviation between the two refinements.

Discussion

The interatomic distances and angles are given in Tables 5, 6, 7 and 8. These values along with their standard deviations were calculated with the Busing, Martin & Levy (1964) program *ORFFE*. Fig. 2 shows a projection of the $LuFeO_3$ structure on the *xy* plane. This compound has the most distorted arrangement among the rare-earth orthoferrites. As can be seen from Table 5 where the Fe–O, O–O distances and O–Fe–O angles

are given, the distortion of the iron octahedra is rather small even in $LuFeO_3$. This distortion decreases on going from Lu to Pr. If one defines an index of distortion as the standard deviation calculated from the twelve edges of the oxygen octahedron, a value of $\sim 1 \times 10^{-2}$ for $LuFeO_3$ is obtained. This value decreases linearly to 4×10^{-3} for $PrFeO_3$. In the cubic perovskite the twelve O–O distances are all the same.

The average Fe–O and O–O distances are almost the same in every orthoferrite. The overall values are 2·011 and 2·844 Å for Fe–O and O–O respectively. In Table 8 the angles Fe–O–Fe are given. These values, which are important for the superexchange interaction, are in good agreement with the values predicted by Coppens & Eibschütz (1965) from geometrical considerations.

The distortion of the oxygen polyhedra around the rare earth ions is very large, even in $PrFeO_3$ which has the least distorted arrangement among the rare-earth orthoferrites described herein [see Fig. 1(*b*)]. In Table 6 the RE–O distances and the O–RE–O angles are given. These angles provide an indication of distortion of the polyhedron around the rare earth. The twelve 90° O–RE–O angles in the cubic perovskite structure vary in the case of $PrFeO_3$ from 113·2 to 72°, whereas in $LuFeO_3$ they vary from 123·0 to 60°.

In Fig. 3(*a*), (*b*) and (*c*) the individual RE–O distances are plotted against the ionic radii of the rare earths (Shannon & Prewitt, 1969). The radii corresponding to C.N. = 8 have been chosen, but, as it will be shown later, this is not a very good approximation after $SmFeO_3$. The first six RE–O distances increase linearly from Lu to Pr. The rate of increase is almost the same for all six distances, *i.e.* $\Delta d/\Delta r \simeq 1$. This behavior indicates that each one of these oxygen atoms is a first-nearest neighbor to the rare earth. The seventh and eight RE–O distances, RE^{ii}–$O(2)^{v}$ and RE^{ii}–$O(2)^{vi}$, decrease on going from Lu to Ho and increase from Dy to Pr. The rate of increase $\Delta d/\Delta r$ is definitely less than that of the first six RE–O distances. This behavior indicates that the two oxygen atoms O^{v} and O^{vi} in the perovskites from Lu to Dy are not truly first-nearest neighbors to the rare earths. It seems that

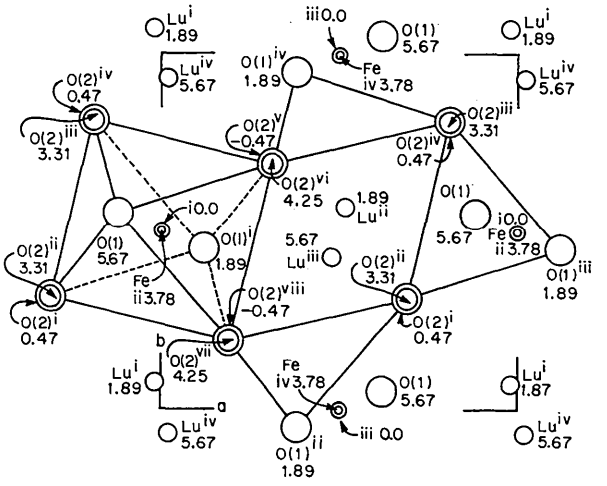

Fig. 2. The projection of one unit cell on the *xy* plane. The heights of the atoms are in ångströms. An oxygen–iron octahedron and an oxygen–rare earth polyhedron are outlined.

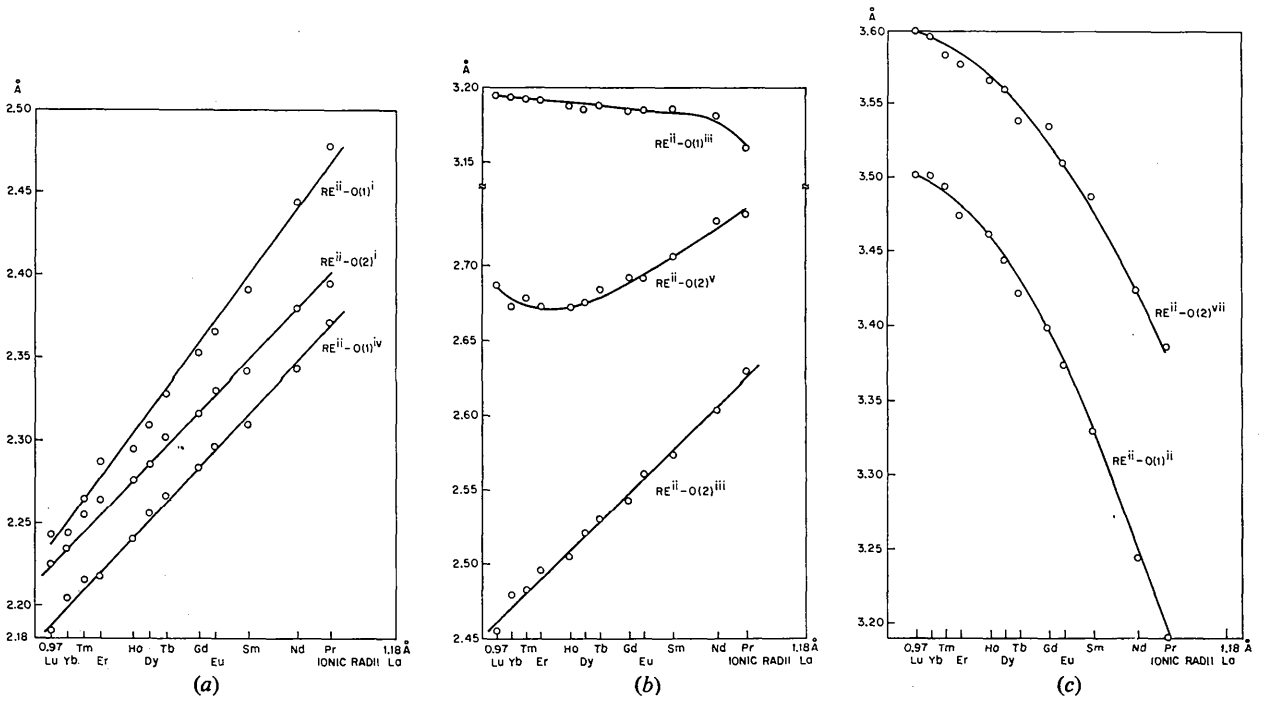

(*a*) (*b*) (*c*)

Fig. 3. The RE–O distances *vs.* ionic radii.

Table 5. *Interatomic distances* (Å) *and angles* (°) *in the iron octahedra*

	Pr	Nd	Sm	Eu	Gd	Tb	Dy	Ho	Er	Tm	Yb	Lu
Fe^{ii}—$O(1)^{i}$	2·001 (1)	2·004 (1)	2·001 (1)	2·000 (1)	2·000 (2)	1·997 (1)	1·998 (1)	1·998 (2)	2·003 (3)	2·005 (2)	2·006 (2)	2·008 (2)
Fe^{ii}—$O(2)^{vi}$	2·015 (3)	2·017 (3)	2·030 (2)	2·029 (3)	2·030 (4)	2·030 (2)	2·033 (3)	2·031 (3)	2·029 (3)	2·026 (3)	2·025 (4)	2·024 (4)
Fe^{ii}—$O(2)^{vii}$	2·010 (3)	2·010 (3)	2·007 (2)	2·010 (3)	2·013 (4)	2·008 (2)	2·004 (3)	2·001 (3)	2·002 (3)	2·003 (3)	2·001 (4)	1·997 (4)
$O(1)^{i}$ —$O(2)^{vii}$	2·826 (5)	2·823 (4)	2·820 (3)	2·809 (4)	2·815 (5)	2·802 (4)	2·802 (3)	2·795 (4)	2·793 (4)	2·787 (4)	2·784 (6)	2·793 (5)
$O(1)^{i}$ —$O(2)^{vi}$	2·864 (5)	2·868 (4)	2·867 (3)	2·868 (4)	2·874 (5)	2·871 (3)	2·870 (4)	2·868 (4)	2·866 (4)	2·880 (5)	2·881 (5)	2·884 (5)
$O(1)^{i}$ —$O(2)^{ii}$	2·806 (5)	2·809 (4)	2·801 (4)	2·802 (4)	2·800 (6)	2·792 (4)	2·790 (4)	2·787 (5)	2·797 (5)	2·787 (5)	2·785 (6)	2·779 (6)
$O(1)^{i}$ —$O(2)^{iii}$	2·854 (5)	2·864 (4)	2·881 (4)	2·889 (4)	2·884 (6)	2·983 (4)	2·898 (4)	2·901 (5)	2·908 (5)	2·913 (6)	2·915 (7)	2·908 (6)
$O(2)^{vi}$ –$O(2)^{vii}$	2·828 (2)	2·834 (2)	2·849 (2)	2·859 (2)	2·865 (2)	2·862 (2)	2·964 (2)	2·861 (2)	2·859 (2)	2·857 (2)	2·852 (2)	2·845 (2)
$O(2)^{vi}$ –$O(2)^{iii}$	2·862 (2)	2·861 (2)	2·860 (2)	2·853 (2)	2·853 (3)	2·849 (2)	2·847 (2)	2·841 (3)	2·841 (3)	2·841 (3)	2·842 (3)	2·842 (3)
$O(1)^{i}$ —Fe^{ii}–$O(2)^{vii}$	89·4 (2)	89·2 (1)	88·8 (1)	88·4 (1)	88·6 (2)	88·2 (1)	88·1 (1)	87·8 (2)	87·7 (1)	87·5 (2)	87·4 (2)	87·7 (2)
$O(1)^{i}$ —Fe^{ii}–$O(2)^{i}$	88·8 (2)	88·8 (1)	88·7 (1)	88·7 (1)	88·5 (2)	88·4 (1)	88·4 (1)	88·4 (2)	88·6 (1)	88·1 (2)	88·1 (2)	87·9 (2)
$O(2)^{vii}$–Fe^{ii}–$O(2)^{vi}$	89·3 (1)	89·5 (1)	89·8 (1)	90·1 (1)	90·2 (1)	90·3 (1)	90·3 (1)	90·4 (1)	90·4 (1)	90·3 (1)	90·2 (1)	90·1 (1)
Average Fe–O	2·009	2·010	2·013	2·013	2·014	2·012	2·012	2·010	2·011	2·011	2·011	2·010
O –O	2·840	2·843	2·846	2·847	2·849	2·845	2·845	2·842	2·844	2·844	2·843	2·842

Table 6. *Interatomic distances* (Å) *and angles* (°) *in the rare-earth polyhedron*

	Pr	Nd	Sm	Eu	Gd	Tb	Dy	Ho	Er	Tm	Yb	Lu
RE^{ii}–$L(1)^{iv}$	2·371 (4)	2·343 (4)	2·310 (3)	2·297 (4)	2·284 (6)	2·267 (4)	2·256 (4)	2·240 (5)	2·217 (4)	2·215 (5)	2·204 (6)	2·185 (5)
–$O(1)^{i}$	2·478 (5)	2·444 (5)	2·391 (4)	2·365 (4)	2·352 (6)	2·329 (4)	2·310 (4)	2·295 (5)	2·287 (4)	2·265 (5)	2·244 (7)	2·243 (5)
–$O(1)^{iii}$	3·160 (4)	3·172 (4)	3·177 (4)	3·176 (4)	3·175 (5)	3·179 (4)	3·176 (4)	3·178 (5)	3·192 (5)	3·193 (5)	3·194 (6)	3·195 (5)
–$O(1)^{ii}$	3·190 (5)	3·244 (5)	3·329 (4)	3·374 (4)	3·399 (6)	3·422 (4)	3·444 (4)	3·462 (5)	3·474 (4)	3·494 (5)	3·502 (7)	3·502 (6)
–$O(2)^{i}$ (2)	2·395 (3)	2·380 (3)	2·342 (2)	2·331 (3)	2·317 (4)	2·302 (3)	2·286 (3)	2·277 (3)	2·264 (3)	2·255 (3)	2·234 (4)	2·225 (4)
–$O(2)^{iii}$ (2)	2·629 (3)	2·603 (3)	2·573 (2)	2·561 (3)	2·543 (4)	2·530 (3)	2·521 (3)	2·505 (3)	2·495 (3)	2·482 (4)	2·478 (4)	2·455 (4)
–$O(2)^{vi}$ (2)	2·730 (3)	2·730 (3)	2·706 (2)	2·692 (3)	2·692 (4)	2·684 (3)	2·676 (3)	2·673 (4)	2·673 (3)	2·679 (4)	2·673 (4)	2·687 (4)
–$O(2)^{vii}$ (2)	3·386 (3)	3·424 (3)	3·487 (2)	3·510 (3)	3·535 (4)	3·539 (3)	3·560 (3)	3·566 (3)	3·577 (3)	3·582 (3)	3·595 (4)	3·599 (4)
$O(1)^{i}$ –RE^{ii}–$O(1)^{iv}$	87·2 (1)	87·3 (1)	87·9 (1)	88·2 (1)	88·3 (1)	88·5 (1)	88·6 (1)	88·6 (1)	88·3 (1)	88·6 (1)	88·6 (2)	88·4 (1)
$O(1)^{iv}$ –RE^{ii}–$O(1)^{iii}$	108·2 (1)	110·0 (1)	112·8 (1)	114·1 (1)	115·0 (2)	116·0 (1)	117·0 (1)	117·9 (1)	118·8 (1)	119·5 (2)	120·3 (2)	120·7 (1)
$O(1)^{iii}$ –RE^{ii}–$O(1)^{ii}$	92·4 (1)	92·1 (1)	91·4 (1)	90·9 (1)	90·8 (2)	90·6 (1)	90·4 (1)	90·3 (1)	90·5 (1)	90·1 (1)	90·2 (2)	90·2 (1)
$O(1)^{ii}$ –RE^{ii}–$O(1)^{i}$	72·2 (1)	70·5 (1)	68·0 (1)	66·7 (1)	65·9 (2)	65·0 (1)	64·1 (1)	63·3 (1)	62·4 (1)	61·7 (2)	61·1 (2)	60·6 (1)
$O(2)^{v}$ –RE^{ii}–$O(2)^{vi}$	113·5 (1)	114·9 (1)	117·3 (1)	118·2 (1)	119·2 (2)	119·6 (1)	120·6 (1)	121·0 (1)	121·6 (1)	121·9 (1)	122·7 (2)	123·0 (1)
$O(2)^{i}$ –RE^{ii}–$O(2)^{ii}$	84·2 (2)	83·4 (2)	82·5 (1)	82·2 (2)	81·5 (2)	81·5 (1)	81·2 (1)	80·8 (2)	80·5 (2)	80·1 (2)	80·2 (2)	79·4 (2)
$O(2)^{i}$ –RE^{ii}–$O(2)^{v}$	80·4 (1)	79·9 (1)	78·7 (1)	78·2 (1)	77·9 (1)	77·8 (1)	77·1 (1)	77·0 (1)	76·8 (1)	76·8 (1)	76·2 (1)	76·4 (1)
$O(2)^{vii}$–RE^{ii}–$O(2)^{viii}$	85·0 (1)	84·4 (1)	83·0 (1)	82·3 (1)	82·1 (1)	81·9 (1)	81·5 (1)	81·4 (1)	81·4 (1)	81·6 (1)	81·5 (1)	82·0 (1)
$O(2)^{iii}$ –RE^{ii}–$O(2)^{iv}$	75·3 (1)	74·9 (1)	73·7 (1)	73·5 (1)	73·0 (2)	72·6 (1)	72ö3 (2)	72·2 (2)	71·8 (1)	71·5 (2)	71·0 (2)	70·8 (2)
$O(2)^{iii}$ –RE^{ii}–$O(2)^{vii}$	99·6 (1)	100·0 (1)	101·2 (1)	101·7 (1)	102·0 (1)	102·3 (1)	102·6 (1)	102·7 (1)	102·9 (1)	102·9 (1)	103·2 (1)	103·1 (1)
$O(2)^{vi}$ –RE^{ii}–$O(2)^{vii}$	53·8 (1)	53·4 (1)	53·0 (1)	52·9 (1)	52·7 (1)	52·6 (1)	52·4 (1)	52·2 (1)	52·0 (1)	51·9 (1)	51·6 (1)	51·3 (1)
$O(2)^{vii}$–RE^{ii}–$O(2)^{ii}$	56·3 (1)	55·6 (1)	54·6 (1)	54·0 (1)	53·6 (1)	53·4 (1)	53·0 (1)	52·7 (1)	52·6 (1)	52·4 (1)	52·2 (1)	52·1 (1)
$O(2)^{ii}$ –RE^{ii}–$O(2)^{iii}$	68·3 (1)	69·2 (1)	70·7 (1)	71·3 (1)	72·1 (1)	72·5 (1)	72·9 (1)	73·3 (1)	73·7 (1)	74·0 (1)	74·3 (1)	74·7 (1)
$O(2)^{iii}$ –RE^{ii}–$O(2)^{vi}$	64·5 (1)	64·8 (1)	65·6 (1)	65·8 (1)	66·0 (1)	66·2 (1)	66·4 (1)	66·5 (1)	66·6 (1)	66·8 (1)	66·9 (1)	66·9 (1)
$O(1)^{i}$ –RE^{ii}–$O(2)^{vii}$	55·5 (1)	54·8 (1)	53·7 (1)	53·0 (1)	52·7 (1)	52·3 (1)	51·9 (1)	51·6 (1)	61·3 (1)	51·1 (1)	50·7 (1)	50·9 (1)
$O(2)^{vii}$–RE^{ii}–$O(1)^{ii}$	51·5 (1)	50·9 (1)	49·7 (1)	49·2 (1)	48·9 (1)	48·7 (1)	48·3 (1)	48·1 (1)	47·9 (1)	48·0 (1)	47·9 (1)	47·9 (1)
$O(1)^{ii}$ –RE^{ii}–$O(2)^{ii}$	59·4 (1)	58·9 (1)	58·0 (1)	57·4 (1)	56·9 (1)	56·8 (1)	56·5 (1)	56·3 (1)	56·2 (1)	56·0 (1)	55·9 (1)	55·8 (1)
$O(2)^{ii}$ –RE^{ii}–$O(1)^{iii}$	58·8 (1)	58·7 (1)	58·7 (1)	58·8 (1)	58·9 (1)	58·7 (1)	58·8 (1)	58·7 (1)	58·8 (1)	58·6 (1)	58·6 (1)	58·5 (1)
$O(1)^{iii}$ –RE^{ii}–$O(2)^{iii}$	58·2 (1)	58·5 (1)	59·0 (1)	59·3 (1)	59·4 (1)	59·6 (1)	59·8 (1)	60·0 (1)	60·0 (1)	60·2 (1)	60·3 (1)	60·3 (1)
$O(2)^{iii}$ –RE^{ii}–$O(1)^{iv}$	66·6 (1)	67·6 (1)	68·6 (1)	69·2 (1)	69·7 (1)	70·0 (1)	70·4 (1)	70·8 (1)	71·4 (1)	71·7 (1)	72·1 (2)	72·4 (1)
$O(1)^{iv}$ –RE^{ii}–$O(2)^{vi}$	65·4 (1)	65·9 (1)	66·9 (1)	67·1 (1)	67·5 (1)	67·5 (1)	67·9 (1)	68·0 (1)	68·0 (1)	68·0 (1)	68·3 (1)	68·3 (1)
$O(2)^{vi}$ –RE^{ii}–$O(1)^{i}$	67·8 (1)	68·4 (1)	69·2 (1)	69·7 (1)	70·0 (1)	70·3 (1)	70·6 (1)	70·8 (1)	71·1 (1)	71·4 (1)	71·7 (1)	71·8 (1)

they become first-nearest neighbors only in $TbFeO_3$. The ninth distance RE^{ii}–$O(1)^{iii}$ decreases very slowly with increasing radius. After Nd it starts to drop quite rapidly (the value of this distance in $LaFeO_3$ is 3·041 Å). This variation indicates that $O(1)^{iii}$ is a second-nearest neighbor to the rare earth. The last three distances, RE^{ii}–$O(1)^{ii}$, RE^{ii}–$O(2)^{vii}$ and RE^{ii}–$O(2)^{viii}$,

Table 7. *Rare earth – iron distances* (Å)

	Pr	Nd	Sm	Eu	Gd	Tb	Dy	Ho	Er	Tm	Yb	Lu
RE^{ii}–Fe^{i}	3·411 (1)	3·406 (1)	3·390 (1)	3·383 (1)	3·377 (1)	3·365 (1)	3·360 (1)	3·351 (1)	3·346 (1)	3·342 (1)	3·335 (1)	3·329 (1)
RE^{ii}–Fe^{iv}	3·604 (1)	3·629 (2)	3·665 (2)	3·682 (2)	3·670 (2)	3·693 (2)	3·701 (1)	3·702 (2)	3·702 (2)	2·701 (2)	3·695 (2)	3·693 (2)
RE^{ii}–Fe^{iii}	3·205 (1)	3·182 (1)	3·143 (1)	3·127 (1)	3·114 (1)	3·101 (1)	3·087 (1)	3·075 (1)	3·065 (1)	3·060 (1)	3·057 (1)	3·039 (1)
RE^{ii}–Fe^{ii}	3·330 (1)	3·311 (1)	3·276 (1)	3·257 (1)	3·242 (1)	3·228 (1)	3·214 (1)	3·199 (1)	3·190 (1)		3·172 (1)	3·162 (1)

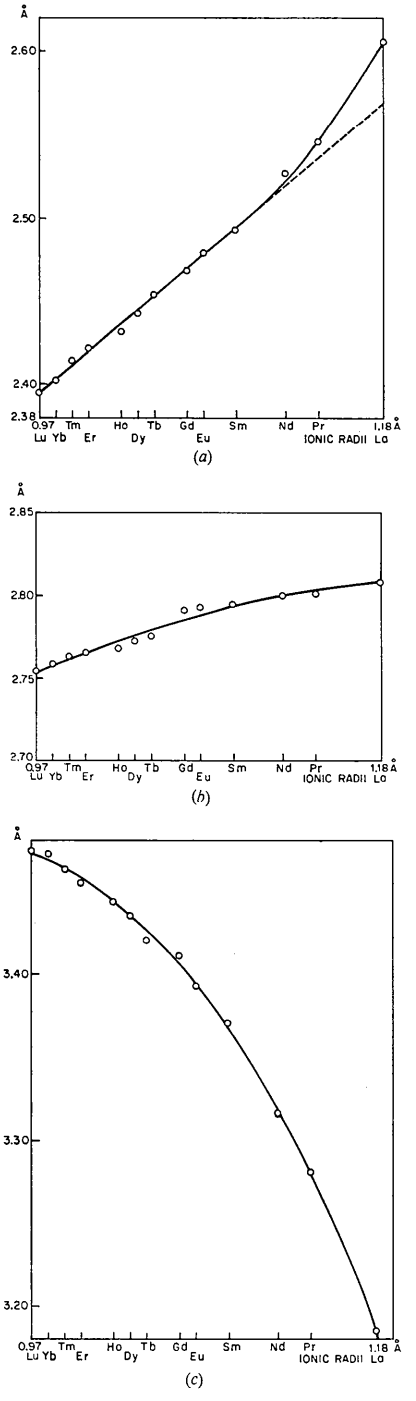

Fig. 4. The average of (*a*) the first eight, (*b*) and (*c*) the last four RE–O distances *vs.* ionic radii.

Table 8. Fe–O–Fe *and* Fe–O-RE *angles*

	Corresponding Fe–O or RE–O distances in $PrFeO_3$		Pr	Nd	Sm	Eu	Gd	Tb
Fe^{ii} –$O(1)^{i}$—Fe^{i}	2·001	2·001	153·3 (2)	151·3 (2)	148·9 (2)	147·8 (2)	140·0 (3)	145·8 (2)
Fe^{ii} –$O(2)^{vii}$–Fe^{iv}	2·015	2·010	152·8 (2)	151·4 (2)	148·8 (1)	148·0 (2)	146·0 (2)	146·4 (1)
Fe^{ii} –$O(1)^{i}$—RE^{i}	2·001	2·371	102·2 (1)	102·9 (1)	103·5 (1)	103·6 (1)	103·9 (2)	104·0 (1)
Fe^{ii} –$O(1)^{i}$—RE^{ii}	2·001	2·478	90·7 (1)	90·8 (1)	90·9 (1)	91·1 (1)	91·0 (2)	91·3 (1)
Fe^{iii}–$O(2)^{vi}$ –RE^{ii}	2·015	2·735	83·4 (1)	82·7 (1)	81·8 (1)	81·7 (1)	81·2 (1)	81·0 (1)
Fe^{ii} –$O(2)^{vi}$ –RE^{ii}	2·010	2·735	90·6 (1)	90·6 (1)	90·8 (1)	90·8 (1)	90·6 (1)	90·5 (1)
Fe^{iii}–$O(2)^{iii}$–RE^{i}	2·010	2·629	86·3 (1)	86·2 (1)	85·7 (1)	85·4 (1)	85·4 (1)	85·4 (1)
Fe^{ii} –$O(2)^{vii}$–RE^{ii}	2·015	2·629	90·6 (1)	90·7 (1)	89·9 (1)	89·6 (1)	89·6 (1)	89·4 (1)
Fe^{iii}–$O(2)^{vii}$–RE^{iv}	2·010	2·395	97·9 (1)	97·6 (1)	97·4 (1)	97·1 (1)	96·7 (1)	96·8 (1)
Fe^{iii}–$O(2)^{ii}$—RE^{ii}	2·015	2·395	109·3 (1)	111·0 (1)	113·7 (1)	115·0 (1)	116·3 (2)	116·8 (1)
			Dy	Ho	Er	Tm	Yb	Lu
Fe^{ii} –$O(1)^{i}$—Fe^{i}	2·001	2·001	145·0 (2)	144·1 (3)	142·7 (2)	142·1 (3)	141·4 (3)	140·7 (3)
Fe^{ii} –$O(2)^{vii}$–Fe^{iv}	2·015	2·010	145·4 (1)	144·9 (2)	144·2 (1)	143·8 (2)	142·8 (2)	142·4 (2)
Fe^{ii} –$O(1)^{i}$—RE^{i}	2·001	2·371	104·2 (1)	104·4 (1)	104·8 (1)	104·7 (1)	104·7 (2)	105·0 (1)
Fe^{ii} –$O(1)^{i}$—RE^{ii}	2·001	2·478	91·2 (1)	91·2 (1)	91·0 (1)	91·3 (1)	91·4 (2)	91·1 (2)
Fe^{iii}–$O(2)^{vi}$ –RE^{ii}	2·015	2·735	80·7 (1)	80·4 (1)	80·1 (1)	79·8 (1)	79·5 (1)	79·0 (1)
Fe^{ii} –$O(2)^{vi}$ –RE^{ii}	2·010	2·735	90·6 (1)	90·4 (1)	90·2 (1)	89·9 (1)	89·9 (2)	89·3 (1)
Fe^{iii}–$O(2)^{iii}$–RE^{i}	2·010	2·629	85·2 (1)	85·3 (1)	85·2 (1)	83·5 (1)	85·0 (1)	85·5 (1)
Fe^{ii} –$O(2)^{vii}$–RE^{ii}	2·015	2·629	89·1 (1)	89·1 (1)	89·1 (1)	89·2 (1)	89·0 (2)	89·3 (1)
Fe^{iii}–$O(2)^{vii}$–RE^{iv}	2·010	2·395	96·8 (1)	96·6 (1)	96·6 (1)	96·5 (1)	96·8 (2)	96·8 (1)
Fe^{iii}–$O(2)^{ii}$—RE^{ii}	2·015	2·395	117·8 (1)	118·4 (1)	119·1 (1)	119·5 (1)	120·2 (2)	120·6 (1)

decrease quite rapidly on going from Lu to Pr, especially after Gd, indicating that $O(1)^{ii}$, $O(2)^{vii}$ and $O(2)^{viii}$ are also second-nearest neighbors to the rare earth. The reason for the distance RE^{ii}–$O(1)^{iii}$ decreasing slowly from Lu to Nd is that $O(1)^{iii}$ does not move toward its cubic position on a straight line.

These results corroborate our explanation of the anomalous variation of the lattice parameter *b* across the series of the rare-earth orthoferrites. The rapid decrease of the three longest distances RE–O after Gd is responsible for the corresponding decrease of the *b* parameter. Also, the results explain why only the *b* parameter has an anomalous variation, whereas the lattice parameters *a* and *c* increase smoothly on going from Lu to Pr.

It is difficult to decide what the value of the coordination number should be as one proceeds across the series. For instance, in $LuFeO_3$ the average of the first eight Lu–O distances is 2·395 Å while the average of the other four is 3·474 Å (see Table 6). The difference between the two averages, 1·079 Å, indicates that it would be a good approximation to assign a coordination number of 8 to the Lu ions. This difference between the average of the first-nearest and the second-nearest neighbors decreases on going to the lighter rare earths: it is 0·732 Å in $PrFeO_3$ and 0·580 Å in $LaFeO_3$. In this last compound the twelve La–O distances are: La–O(1) = 2·416 (4), 2·591 (6), 3·041 (6), 3·156 (5) Å, La–O(2) × 2 = 2·455 (4), 2·656 (4), 2·805 (4), 3·271 (4) Å. The difference between the eighth value, 2·805 Å, and the ninth, 3·041 Å, is not large enough, 0·236 Å, to justify the assumption that the La ions have an eightfold coordination. In Fig. 4(*a*) the average of the first eight RE–O distances (including $LaFeO_3$) are plotted *versus* the ionic radii of the rare earths with C.N. = 8. In Fig. 4(*b*) and (*c*), the averages of all twelve RE–O distances and of the remaining four distances are respectively plotted. The curve corresponding to the average of the first eight RE–O distances can be divided approximately into two linear parts with two different slopes: one from Lu to Sm and the second from Sm to La. Only one plausible explanation can be found for the fact the latter section has a steeper slope than the former. Our results seem to indicate that after Sm the approximation that the rare earths have C.N. = 8 is no longer valid, and it would appear that larger values for the ionic radii would be more appropriate.

From our data it is now possible to make some general statements about the crystal chemistry of some isostructural compounds. An interesting structure to consider is $InCrO_3$ which under 65 kbar pressure can be synthesized with the orthorhombic perovskite-like structure. The In atoms occupy the rare-earth sites and the Cr atoms the octahedral sites. The ionic radius of In^{3+} with C.N. = 8 is 0·92 Å. From the variations of the interatomic distances reported in Fig. 3(*a*), (*b*) and (*c*), one can extrapolate that in the structure of a hypothetical $InFeO_3$ with the perovskite-like arrangement the 12 In–O distances would be: In–O(1) = 2·12, 2·16, 3·21, 3·53 Å and In–O(2) × 2 = 2·16, 2·39, 2·73, 3·62 Å. We believe that these would also be the values of the In–O distances in the compound $InCrO_3$. The oxygen octahedra around the iron or the chronium atoms should be as distorted as the oxygen octahedra around the iron atoms in the rare-earth orthoferrites. As was stated above, from Ho to Lu the seventh and eighth oxygen atoms of the polyhedra around the rare earths are beginning to behave as second-nearest neighbors, in fact the corresponding distances increase on going from Ho to Lu. These oxygen atoms should be further removed from the indium atoms in $InCrO_3$ than from the Lu atoms in $LuFeO_3$. It should still be a good approxima-

tion to assume that the indium atoms have an eightfold coordination.

Shannon (1967) reported the synthesis of the rare earth indates $REInO_3$ with the perovskite-like structure; the synthesis was done at 65 kbar and 1000° C. $InCrO_3$ was synthesized under the same conditions of pressure and temperature. Therefore, the indium atoms can occupy the *A* or the *B* sites in the perovskite-like compounds. Indium sesquioxide has been reported to crystallize with two structures: at atmospheric pressure it crystallizes with the *C* phase of the rare-earth sesquioxides whereas at high pressure it crystallizes with the corundum structure (Christensen, Broch, Heidenstam & Nilson, 1967; Prewitt, Shannon, Rogers & Sleight, 1969). It can be speculated that at higher pressures In_2O_3 could crystallize with a perovskite-like structure. Recently one of us has observed the transformation corundum → perovskite in $InGaO_3$ under pressure (Marezio, 1969). This compound can crystallize with four different phases by varying the pressure at which the synthesis is carried out. The data of this polymorphism are summarized in the following table:

	$In^{VI}Ga^{IV}O_2^{III}O^{IV}$	→	$In^{VI}Ga^{V}O^{III}O_2^{IV}$	→	$In^{VI}Ga^{VI}O_3^{IV}$	→	$In^{VIII}Ga^{VI}O^{IV}O_2^{V}$
Structure	β-Ga_2O_3		*		α-Al_2O_3		$GdFeO_3$
Symmetry	Monoclinic		Hexagonal		Trigonal		Orthorhombic

* Shannon & Prewitt (1968).

The authors would like to thank Dr A. Santoro for helpful discussion, Mrs R. C. Fulton for her assistance in programming and Mr E. M. Kelly for his assistance in crystal growth.

References

BERTAUT, E. F. & FORRAT, F. (1956). *J. Phys. Radium*, **17**, 129.

BUSING, W. R., MARTIN, K. O. & LEVY, H. A. (1964). ORNL Report TM-306, Oak Ridge National Laboratory, Oak Ridge, Tennessee.

CHRISTENSEN, A. N., BROCH, N. C., HEIDENSTAM, O. V. & NILSSON, A. (1967). *Acta Chem. Scand.* **21**, 1046.

COPPENS, D. T. & EIBSCHÜTZ, M. (1965). *Acta Cryst.* **19**, 524.

CROMER, D. T. (1965). *Acta Cryst.* **18**, 17.

CROMER, D. T. & WABER, J. T. (1965). *Acta Cryst.* **18**, 104.

EIBSCHÜTZ, M. (1965). *Acta Cryst.* **19**, 337.

GELLER, S. (1956). *J. Chem. Phys.* **24**, 1236.

MAREZIO, M. (1969). *Trans. Amer. Cryst. Assoc.* p. 29.

MAREZIO, M., REMEIKA, J. P. & DERNIER, P. D. (1968). *Inorg. Chem.* **7**, 1337.

MAREZIO, M., REMEIKA, J. P. & DERNIER, P. D. (1970). *Acta Cryst.* B**26**, 300.

MUELLER, M. H., HEATON, L. & MILLER, R. T. (1960). *Acta Cryst.* **13**, 828.

PREWITT, C. T. (1966*a*). Unpublished computer program for crystallographic least-squares refinement.

PREWITT, C. T. (1966*b*). Unpublished computer program for absorption correction.

PREWITT, C. T., SHANNON, R. D., ROGERS, D. B. & SLEIGHT, A. W. (1969). *Inorg. Chem.* **8**, (9), 1985.

REMEIKA, J. P. & KOMETANI, T. Y. (1968). *Mater. Res. Bull.* **3**, 895.

SHANNON, R. D. (1967). *Inorg. Chem.* **6**, 1474.

SHANNON, R. D. & PREWITT, C. T. (1968). *J. Inorg. Nucl. Chem.* **30**, 1389.

SHANNON, R. D. & PREWITT, C. T. (1969). *Acta Cryst.* B**25**, 925.

ZACHARIASEN, W. H. (1963). *Acta Cryst.* **16**, 1139.

Acta Cryst. (1970). B**26**, 2022

Die Kristallstruktur von Amyrolin – Seselin ($C_{14}H_{12}O_3$)

VON KATSUO KATO

Mineralogisch-Petrographisches Institut der Universität Hamburg, Deutschland

(*Eingegangen am* 24. *September* 1969 *und wiedereingereicht am* 16. *Januar* 1970)

Amyrolin ($C_{14}H_{12}O_3$), identical with seselin, crystallizes in the space group $P2_1/c$ with unit-cell dimensions $a=8{\cdot}428$, $b=11{\cdot}112$, $c=12{\cdot}328$ Å and $\beta=103{\cdot}14°$; $Z=4$. The structure was derived mainly by consideration of Patterson maps and molecular packing. The direct method was also applied. The least-squares refinement including hydrogen atoms led to the final value of R 0·061 based on 1617 counter data.

Einführung

Soden & Rojahn (1900) isolierten Amyrolin aus verseiftem west-indischem Sandelholzöl. Nach ihren Angaben schmilzt es bei 117°C, hat die Zusammensetzung $C_{14}H_{12}O_3$, enthält keine Methoxylgruppe und scheint ein der aromatischen Reihe angehöriger laktonartiger Körper zu sein.